Atmospheric
Measurement
Techniques
Discussions

Open Access

EGU

A new method to quantify particulate sodium and potassium salts (nitrate, chloride, and sulfate) by thermal desorption aerosol mass spectrometry

Yuya Kobayashi and Nobuyuki Takegawa

Department of Chemistry, Graduate School of Science, Tokyo Metropolitan University, Hachioji, Tokyo 192-0397, Japan

Correspondence to: Nobuyuki Takegawa (takegawa@tmu.ac.jp)

Abstract. The reaction of sea salt (or biomass burning) particles with sulfuric acid and nitric acid leads to the displacement of chloride relative to sodium (or potassium). We have developed a new particle mass spectrometer to quantify non-refractory and refractory sulfate aerosols (referred to as refractory aerosol thermal desorption mass spectrometer: rTDMS). The combination of a graphite particle collector and a carbon dioxide laser enables high desorption temperature (up to 930°C). Ion signals originating from evolved gas molecules are detected by a quadrupole mass spectrometer. Here we propose a new method to quantify the mass concentrations of sodium nitrate ($NaNO_3$: SN), sodium chloride (NaCl: SC), sodium sulfate (Na_2SO_4: SS), potassium nitrate (KNO_3: PN), potassium chloride (KCl: PC), and potassium sulfate (K_2SO_4: PS) particles by using the rTDMS. Laboratory experiments were performed to test the sensitivities of the rTDMS to various types of particles. We measured ion signals originating from single-component particles for each compound, and found a good linearity ($r^2 > 0.8$) between the major ion signals and mass loadings. We also measured ion signals originating from internally mixed SN + SC + SS (or PN + PC + PS) particles, and found that the temporal profiles of ion signals at m/z 23 (or 39) were characterized by three sequential peaks associated with the evolution of the desorption temperature. We tested potential interferences in the quantification of sea salt particles under real-world conditions by artificially generating "modified" sea salt particles from a mixture of diluted seawater and SS/SN solution. Based on these experimental results, the applicability of the rTDMS to ambient measurements of sea salt particles is discussed.

1 Introduction

Aerosols have large impacts on the Earth's radiation budget by scattering and absorbing solar short-wave radiation (direct effect) and by acting as cloud condensation nuclei (indirect effect) (IPCC 2013). The size and chemical composition of aerosol particles are important for quantitatively estimating the direct and indirect effects of aerosols. Aerosol particles emitted from sea spray and biomass burning make significant contributions to the global budget of aerosols. The reaction of sea salt (or biomass burning) particles with sulfuric acid (H_2SO_4) and nitric acid (HNO_3) leads to the displacement of chloride relative to sodium (or potassium). Sea salt aerosols generally make the largest contribution to the budget of natural aerosols in the troposphere (Seinfeld and Pandis, 2006; IPCC, 2013). Significant conversion of sodium chloride (NaCl: SC) to sodium sulfate

Atmospheric
Measurement
Techniques
Discussions

(Na_2SO_4: SS) or sodium nitrate ($NaNO_3$: SN) can take place via the reactions with sulfuric acid (H_2SO_4) or nitric acid (HNO_3) in polluted air exported from urban areas to coastal regions (Kerminen et al., 1998; Hsu et al., 2007; AzadiAghdam et al., 2019). Biomass burning also makes large contributions to the global budget of soot, organics, and inorganic compounds (Andreae and Merlet, 2001; Akagi et al., 2011; Song et al., 2018). Significant conversion of potassium chloride (KCl: PC) to

35 potassium sulfate (K_2SO_4: PS) or potassium nitrate (KNO_3: PN) can also take place via the reactions with H_2SO_4 or HNO_3 when smoke from biomass burning mixes with urban pollution (Li et al., 2003; Zauscher et al., 2015; Schlosser et al., 2017).

Earlier studies investigated the chemical transformation of Cl^- to SO_4^{2-} or NO_3^- in sea salt or biomass burning particles by offline transmission electron microscopy (TEM) and X-ray spectrometry (Miura et al., 1991; Li et al., 2003; Adachi et al., 2015). Single-particle mass spectrometry was also used to qualitatively detect the chemical transformation of

40 Cl^- to SO_4^{2-} and NO_3^- (Hayes et al., 2013). As briefly reviewed by Kobayashi et al. (2021), currently available techniques for online quantitative measurements of aerosols, including a particle-into-liquid-sampler coupled with ion chromatography (PILS-IC; Weber et al., 2001) and an Aerodyne aerosol mass spectrometer (AMS; Jayne et al., 2000), are not optimized for separate quantification of refractory and non-refractory aerosols. Note that the definition of "non-refractory" and "refractory" compounds in atmospheric aerosols is rather empirical and depends on the analysis method. Following the definition by

45 Kobayashi et al. (2021), chemical compounds with a bulk thermal desorption temperature lower than ~673 K are referred to as non-refractory compounds, and the others are referred to as refractory compounds.

The primary purpose of Kobayashi et al. (2021) was to develop a new instrument to quantify refractory and non-refractory sulfate aerosols, which was referred to as a refractory aerosol thermal desorption mass spectrometer (rTDMS). The goal of this study is to develop a new method to quantify particulate sodium and potassium salts (nitrate, chloride, and sulfate)

50 by using the rTDMS. Potential application to sea salt aerosols is also discussed.

2 Experimental

2.1 Instrument description

The concept and operation procedures of the rTDMS were described in detail by Kobayashi et al. (2021), and thus only the key points are presented here. The configuration is similar to that of the particle trap - laser desorption mass

55 spectrometer (PT-LDMS) (Takegawa et al., 2012). The major difference between the rTDMS and PT-LDMS is the structure of the particle collector and laser power. The main components of the rTDMS include an aerodynamic lens (ADL), a graphite particle collector, a quadrupole mass spectrometer (QMS) equipped with a cross-beam type electron ionization (EI) source (QMG700, Pfeiffer Vacuum), and a continuous wave focused CO_2 laser (wavelength: 10.6 μm, ULR-25, Universal Laser Systems). Aerosol particles are introduced into a vacuum chamber via the ADL and collected on the graphite collector. During

60 particle loadings with the inlet valve open, the graphite collector faces the direction toward the inlet. After particles are collected, the graphite collector turns to the opposite direction so that it faces the ionizer of the QMS. The collected particles are vaporized by the CO_2 laser, and evolved gas molecules are detected using the QMS. The blackbody equivalent temperature

Atmospheric
Measurement
Techniques

Open Access

EGU

Discussions

of the outer surface of the graphite collector was measured using a radiation thermometer (Impac IGA 140, LumaSense Technologies, Inc.). The focused CO_2 laser coupled with the graphite collector is the key component of the rTDMS which

65 enables a high desorption temperature (blackbody equivalent temperature of up to 930°C) and a fast increase of the temperature (less than 60 s to reach the maximum temperature from room temperature). The distance between the graphite collector and the ionizer was shortened to 25 mm from 50 mm as compared to that in Kobayashi et al. (2021), which increased the sensitivity by a factor of two to three.

The rTDMS was operated with total measurement cycles ranging from 6 to 8 min, including the time for particle

70 collection (2–4 min), laser irradiation and ion detection (2 min), and cooling of the graphite collector (2 min). The graphite collector was automatically rotated to set the position by using an electronic actuator. The sample was irradiated by the CO_2 laser for a duration of 60 s. The inlet valve was kept closed for 4 min during the laser desorption analysis and cooling. Kobayashi et al. (2021) employed a constant laser power (~20 W) for the detection of non-refractory and refractory sulfate. In this study we tested a two-step laser modulation for better separation of multi-component aerosol particles. Details of the laser

75 power settings are described in Sect. 3.1 and the Supplement.

2.2 Laboratory experiments

The experimental apparatus is basically the same as that presented by Kobayashi et al. (2021). The particle generation system included an air compressor, a Collison atomizer (Model 3076, TSI, Inc.), a diffusion dryer (Model 3062, TSI, Inc.), and a differential mobility analyzer (DMA; Model 3080, TSI, Inc.). A condensation particle counter (CPC; Model 3022A, TSI,

80 Inc.) and the rTDMS were connected downstream of the particle generation system. We set the mobility diameter at 200 nm to generate monodisperse particles. The mass loadings of monodisperse aerosol particles were calculated from the CPC data with corrections for multiply-charged particles (Takegawa and Sakurai, 2011) to derive the instrument sensitivity to various types of particles. Particle-free air (zero air: ZA) was introduced into the rTDMS and CPC to correct for blank levels and also for evaluating potential artifacts.

85 The chemical compounds tested in this study are summarized in Table 1. The main test particles included single-component SN, SC, SS, PN, PC, and PS particles, internally mixed multi-component SN + SC + SS and PN + PC + PS particles with a molar ratio of 1:1:1, and laboratory-generated sea salt particles. Ammonium nitrate (NH_4NO_3: AN), ammonium chloride (NH_4Cl: AC), and ammonium sulfate (($NH_4)_2SO_4$: AS) particles were also used for evaluating the interference from ammonium salts. The results of the measurements of externally-mixed ammonium salt particles are shown in the Supplement.

90 Under real-world conditions, interferences from coexisting compounds should be carefully considered. Regarding sea salt aerosols, this can be achieved by using seawater samples for generating calibration particles. We sampled seawater from Tokyo Bay and prepared a diluted solution (by a factor of 100; equivalent to 4.5 mM of NaCl). The diluted sea water was used for generating pure sea salt particles. We also added SN and SS into the diluted seawater to prepare samples for the standard addition method. A list of the tested solutions is summarized in Fig. 1. This experiment aimed to investigate the quantification

95 of SN and SS in the presence of unidentified compounds in seawater. Estimation of the molar concentrations of various salts

Atmospheric
Measurement
Techniques
Discussions

in the seawater sample is described in the Supplement. Regarding biomass burning aerosols, it is not straightforward to generate combustion particles with reasonable reproducibility. Therefore, we only performed the experiments with authentic standard materials containing potassium.
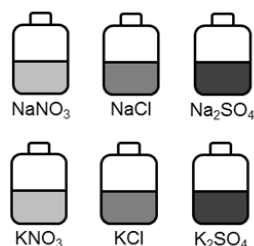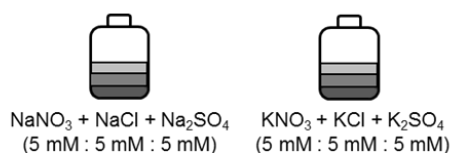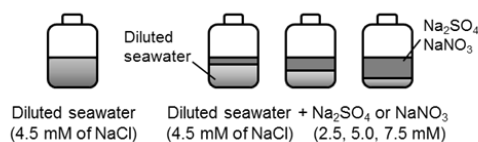

Figure 1. List of tested solutions. (a) Single-component solution of $NaNO_3$ (SN), NaCl (SC), Na_2SO_4 (SS), KNO_3 (PN), KCl (PC), and K_2SO_4 (PS) with a molar concentration of 5 mM. (b) Multi-component solutions of $NaNO_3$ + NaCl + Na_2SO_4 and KNO_3 + KCl + K_2SO_4 with a molar ratio of 1:1:1 (5 mM : 5 mM : 5 mM). (c) Diluted seawater (by a factor of 100; equivalent to 4.5 mM of NaCl) and diluted seawater with Na_2SO_4 or $NaNO_3$ with molar concentrations of 2.5, 5.0, and 7.5 mM.

100

105

110

4

Atmospheric
Measurement
Techniques
Discussions

115 **Table 1.** Chemical compounds tested in this study.

Compound	Abbreviation	Density (g cm^{-3})	Bulk decomposition temperature (°C)
NaNO$_3$	SN	2.26	491
NaCl	SC	2.16	800
Na$_2$SO$_4$	SS	2.66	850
KNO$_3$	PN	2.11	526
KCl	PC	1.98	780
K$_2$SO$_4$	PS	2.66	907–1395
NH$_4$NO$_3$	AN	1.72	142–300
NH$_4$Cl	AC	1.53	220–360
(NH$_4$)$_2$SO$_4$	AS	1.77	250–500

The values of density were taken from Chemical Dictionary (1998). The bulk decomposition temperatures were taken from Broström et al., 2013; Tagawa, 1987; Nakamura et al., 1980; and Tatykaev et al., 2014. The data for ammonium salts are only shown in the Supplement.

2.3 Data analysis

120   The equations for calculating the mass loadings for each compound i, W_i, are the same as those presented by Kobayashi et al. (2021) for both the single-component and multi-component experiments. The effects of hydrated water should be properly considered for the calculations. The relative humidity (RH) downstream of the diffusion dryer was ~5%. Previous studies showed that the efflorescence RHs (ERHs) were 43, 56, 59, and 60% for SC, SS, PC, and PS particles, respectively (Seinfeld and Pandis, 2006; Freney et al., 2009). We assumed that these compounds were effloresced to form solid crystals before
125 reaching the DMA. Previous studies also reported that nitrate particles did not exhibit clear ERH features (e.g., Freney et al., 2009; Lee and Hsu, 2000). We assumed that SN and PN particles lost a majority of water molecules in order to calculate the mass of particles. The particle collection efficiencies of these particles might be higher than those of solid crystal particles.

    Kobayashi et al. (2021) showed that the collection efficiency for solid sulfate particles was ~70%. We did not measure collection efficiencies for various types of particles but assumed that the particle collection efficiency was 100% for all the
130 compounds tested in this study. We considered possible variability in the particle collection efficiencies as systematic uncertainties. For SC, SS, PC, and PS particles, we estimated that the systematic uncertainty due to the collection efficiency was 30% (i.e., the difference between 100% and 70%). For SN and PN particles, we estimated that the systematic uncertainty was 15% because the particle collection efficiency for non-crystal particles would be in the range of 70–100% (85% as the mid point).

135   Temporal profiles of ion signals at selected m/z were integrated over the laser irradiation time to obtain the integrated ion signals for each compound i, $Q_{m/z,i}$. The major m/z values for each compound are listed in Table 2. Variations in $Q_{m/z,i}$ due to

drifts in the detector sensitivity were corrected by using m/z 14 (N^+) signals. The sensitivity of the rTDMS at m/z to compound i, $S_{m/z,i}$, is defined as the ratio of $Q_{m/z,i}$ to W_i.

Table 2. Major m/z signals for each compound.

	m/z
SN	23 (Na^+), 30 (NO^+)
SC	23 (Na^+), 36 ($H^{35}Cl^+$)
SS	23 (Na^+), 48 (SO^+)
PN	30 (NO^+), 39 (K^+, $C_3H_3^+$)
PC	36 ($H^{35}Cl^+$), 39 (K^+, $C_3H_3^+$)
PS	39 (K^+, $C_3H_3^+$), 48 (SO^+)

3 Results

3.1 Single-component particles

Figure 2 shows temporal profiles of ion signals at m/z 23 (Na^+), 30 (NO^+), 36 ($H^{35}Cl^+$), 39 (K^+, $C_3H_3^+$), 48 (SO^+), and 64 (SO_2^+) originating from monodisperse SN, SC, SS, PN, PC, and PS particles with mobility diameters of 200 nm. As described earlier, we used a two-step laser modulation for better separation of multi-component aerosol particles. We tested various combinations of laser power settings (power and duration time), as described in the Supplement. The power setting and duration of the first step were 7.5 W and 40 s, and those of the second step were 20 W and 20 s. Note that these laser power values were not measured ones but estimated from the product specifications.

Ion signals at m/z 30 originating from SN particles exhibited a distinct peak at the elapsed time of 7–12 s, whereas those at m/z 23 exhibited bimodal broad peaks at 7–12 s and 15–50 s (Fig. 2a). Ion signals at m/z 23 and 36 originating from SC particles exhibited a single peak starting at ~8 s with significant tailing up to ~30 s (Fig. 2b). Ion signals at m/z 23, 48, and 64 from SS particles showed a distinct single peak at 40–52 s (Fig. 2c). Following the discussion by Kobayashi et al. (2021), the fragment ratio of m/z 48 to 64 suggests that the major thermal decomposition product from SS particles was SO_2.

Ion signals at m/z 30 originating from PN particles exhibited a distinct peak at 6–13 s, whereas those at m/z 39 exhibited bimodal broad peaks at 6–13 s and 40–50 s (Fig. 2d). Ion signals at m/z 36 and 39 originating from PC particles exhibited a single peak starting at ~8 s with significant tailing up to ~30 s (Fig. 2e). Ion signals at m/z 39 and 48 from PS particles showed small increases at ~30 s followed by a distinct peak at 40–47 s (Fig. 2f). Similarly to SS, the fragment ratio of m/z 48 to 64 suggests that the major thermal decomposition product from PS particles was SO_2 (not shown). The timing of the ion signals was qualitatively consistent with the order of the bulk thermal decomposition temperature (Table 1).

Atmospheric
Measurement
Techniques
Discussions

Figure 3 shows scatterplots of integrated ion signals versus the mass loadings of the corresponding parent compounds for single-component SN, SC, SS, PN, PC, and PS particles. Data obtained on different days are collectively plotted. The time window for the ion signal integration was set at 5–15 s (at m/z 30) and 5–50 s (at m/z 23, 39) for SN and PN, 5–40 s for SC and PC, 40–55 s for SS, and 30–50 s for PS. There was no systematic difference in the $Q_i - W_i$ relationship between the data obtained on different days, and the correlation coefficients were generally high ($r^2 > 0.8$) for all the compounds tested, indicating good linearity and reproducibility in detecting these compounds. The scatter in the m/z 39 signals at mass loadings of zero (i.e., ZA measurements) might be due to interference from organic compounds ($C_3H_3^+$).

The difference in the regression slopes at a specific m/z between different compounds can be interpreted as the variability in the sensitivity with respect to the difference in the chemical form. The regression slope at m/z 30 was 49 and 60 (average of 55) pC per ng of NO_3^- for SN and PN, respectively. The regression slope at m/z 36 was 12 and 17 (average of 15) pC per ng of Cl^- for SC and PC, respectively. As mentioned earlier, the ion fragment ratios of m/z 48 to 64 suggest that the major thermal decomposition products for SS and PS were SO_2, and we used m/z 48 as a representative ion signal for these sulfate compounds. The regression slope at m/z 48 was 5.5 and 5.1 (average of 5.3) pC per ng of SO_4^{2-} for SS and PS, respectively. These results suggest that the variability in the sensitivity was less than ~20% for NO_3^-, Cl^-, and SO_4^{2-}. By contrast, the regression slope at m/z 23 was 24, 16, and 8.6 (average of 16) pC per ng of Na for SN, SC, and SS, respectively, and the regression slope at m/z 39 was 30, 21, and 5.0 (average of 19) pC per ng of K for PN, PC, and PS, respectively. These results suggest that the variability in the sensitivity was considerably large for Na and K (more than ~50%).

3.2 Multi-component particles

Figure 4 shows the temporal evolution of ion signals at m/z 23, 30, 36, and 39 originating from internally mixed, multi-component sodium and potassium salt particles with a molar ratio of 1:1:1. The multi-component ion signals at m/z 23 and 39 exhibited trimodal peaks, with the first and second ones partially overlapped. Based on the comparison with the single-component experiment data, the first, second, and third peaks can be attributed to nitrate (SN, PN), chloride (SC, PC), and sulfate (SS, PS), respectively. These results indicate that the temporal profiles of ion signals at m/z 23 (or 39) originating from internally mixed SC + SS + SN (or PC + PS + PN) particles were characterized by three sequential peaks associated with the evolution of the desorption temperature. Note that the third peak at m/z 23 and 39 might be affected by the tails of the ion signals originating from SN and PN particles.

Atmospheric
Measurement
Techniques
Open Access
Discussions
EGU
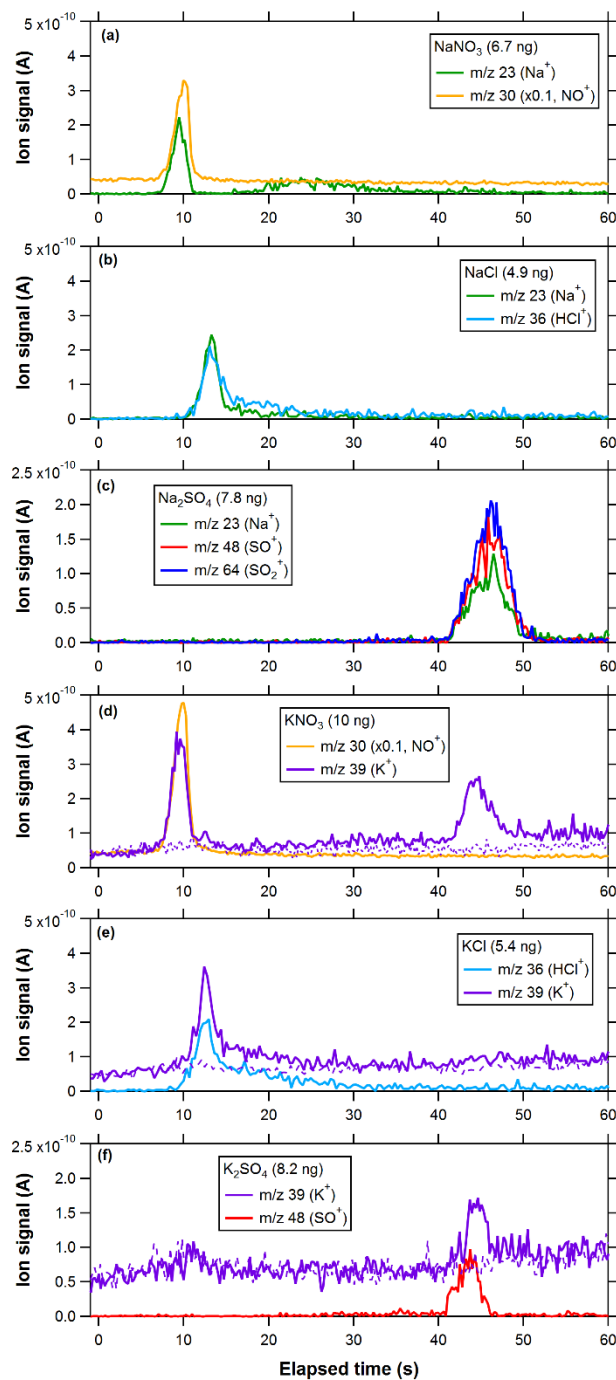
Figure 2. Temporal profiles of ion signals originating from single-component (a) SN, (b) SC, (c) SS, (d) PN, (e) PC, and (f) PS particles as a function of elapsed time since turning the laser on. Zero air signals at *m/z* 39 are also plotted in (d)–(f). Zero signals at *m/z* 23, 30, 36, 48, and 64 are not displayed because the signal levels were comparable to the baselines (i.e., ion signals before the laser irradiation). Particle mass loadings (in ng) are shown in the legend. The elapsed time may contain an error of ~1 s because the laser operation was performed manually.
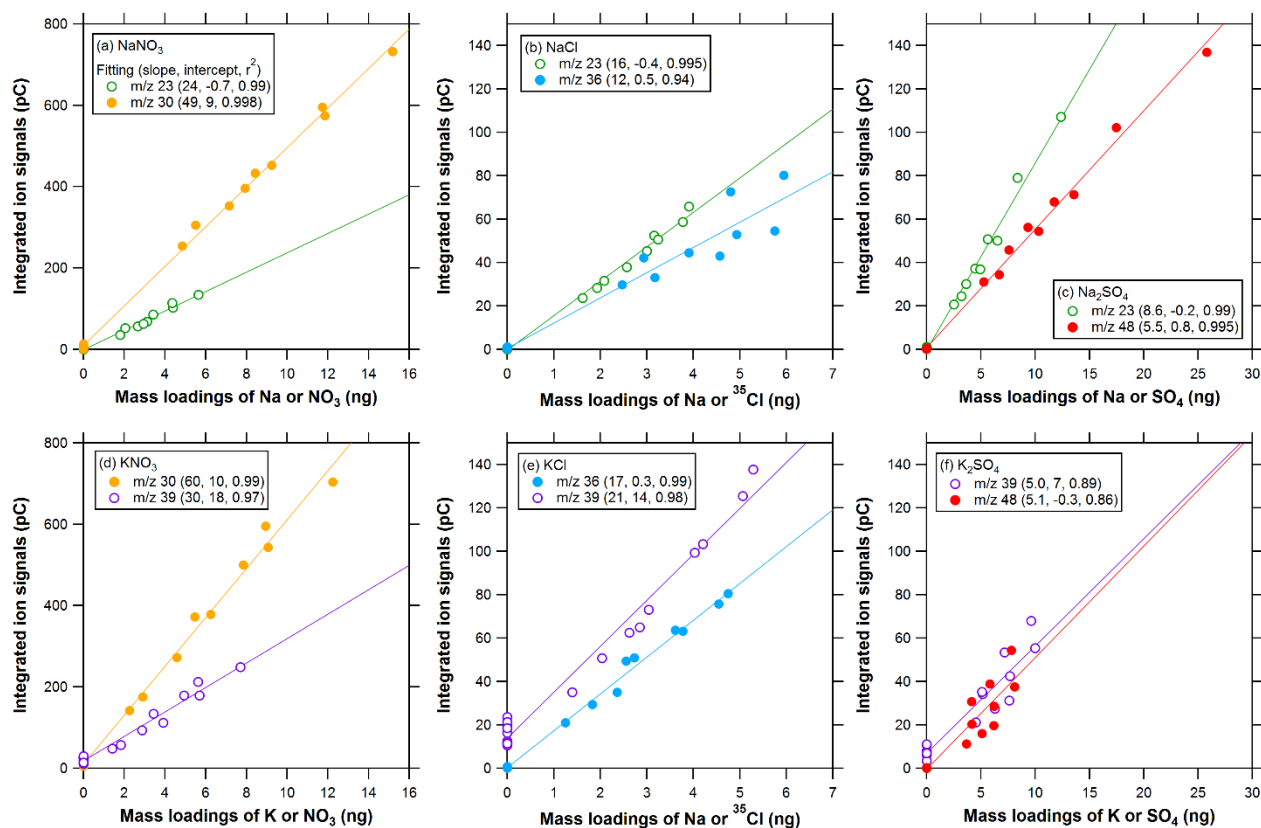
195

Figure 3. Scatterplots of integrated ion signals versus mass loadings (Na for *m/z* 23; K for *m/z* 39; NO$_3$ for *m/z* 30; ^{35}Cl for *m/z* 36; SO$_4$ for *m/z* 48) for (a) SN, (b) SC, (c) SS, (d) PN, (e) PC, and (f) PS particles. The slope, intercept, and r^2 values for the linear regression are indicated in the legend.
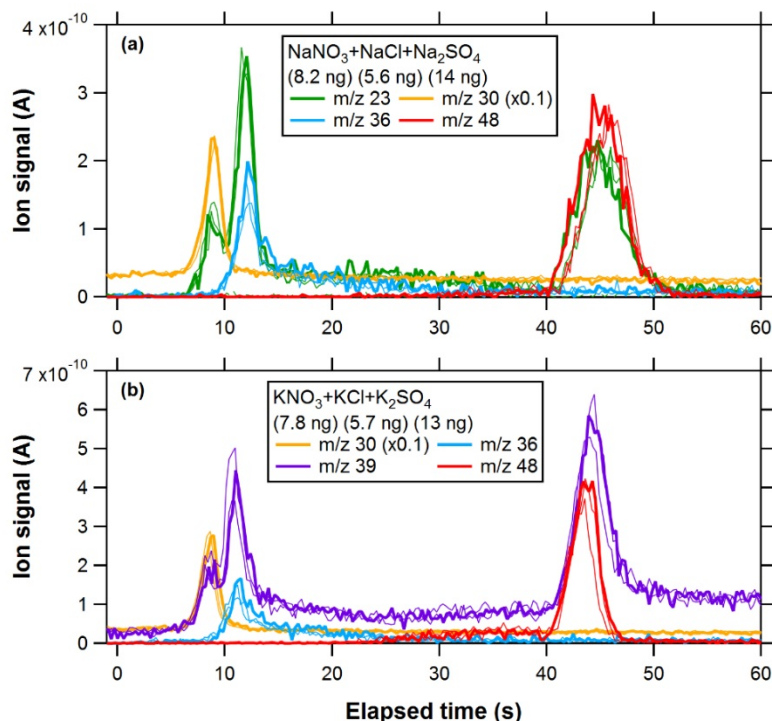
Figure 4. Temporal profiles of ion signals originating from an internal mixture of (a) SN + SC + SS and (b) PN + PC + PS particles. Thin lines represent repeated measurement data normalized to the mass loadings of the main data (thick line).

3.3 Particles generated from seawater samples

Figures 5a–c show the temporal evolution of ion signals at m/z 23, 30, 36, and 48 originating from pure seawater and "seawater + SS/SN" particles. The ion signals at m/z 23 and 36 originating from pure seawater particles exhibited temporal evolution shapes similar to those of the single-component SC particles. Ion signals at m/z 23 originating from seawater + SN particles exhibited partially overlapped bimodal peaks.

Let MX be a salt formed from M^+ and X^- ions. We define the equivalent molar concentration of MX in the seawater sample as the molar concentration of M^+ (or X^-) that would form MX by complete dehydration (see the Supplement for details). Figure 6 shows scatterplots of the molar ratios of SN (or SS) to SC in collected particles estimated from ion signals versus the equivalent molar ratios of SN (or SS) to SC in the solutions. The data points for the authentic multi-component particles described in Sect. 3.2 are also plotted for comparison. The molar ratios of SN (or SS) to SC in the collected particles were calculated using the integrating ion signals at m/z 30 (or 48) and 36. We also used ion signals at m/z 23 to calculate the molar ratios of SN (or SS) to SC in collected particles. We employed a multi-peak fitting method to estimate the contributions of SN and SC to the measured ion signals at m/z 23 (see the Supplement). The linear regression slopes for the seawater + SN particles were found to be 0.38 (by m/z 23) and 0.88 (by m/z 30 and 36), and those for the seawater + SS particles were found to be 1.0

(by m/z 23) and 1.1 (by m/z 36 and 48). The data for the seawater + SN (or SS) samples showed a good linearity ($r^2 \geq 0.98$)

and agreed well with the data points for the authentic multi-component particles, suggesting that interferences of unidentified

220   compounds in seawater were small. The SS/SC ratios estimated from the ion signals at m/z 23 and 48 agreed well with those

predicted from the solution concentrations to within ~10%. The SN/SC ratios estimated from the ion signals at m/z 30 also

agreed well with those predicted from the solution concentrations to within ~10%, whereas the SN/SC ratios estimated from

the ion signals at m/z 23 were systematically lower than those predicted from the solution concentrations. Possible causes for

the difference will be discussed in Sect. 4.3.

225
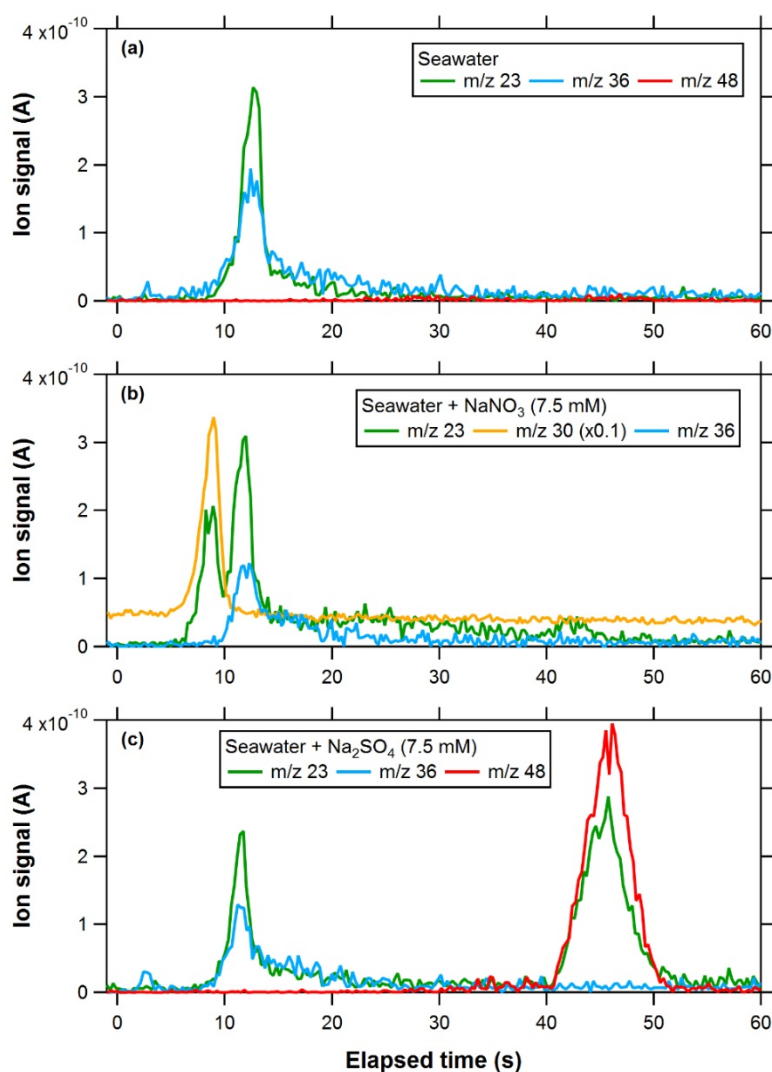
Figure 5. Temporal profiles of ion signals originating from (a) seawater (equivalent to 4.5 mM of SC), (b) seawater + SN (7.5 mM), and (c) seawater + SS (7.5 mM) particles.
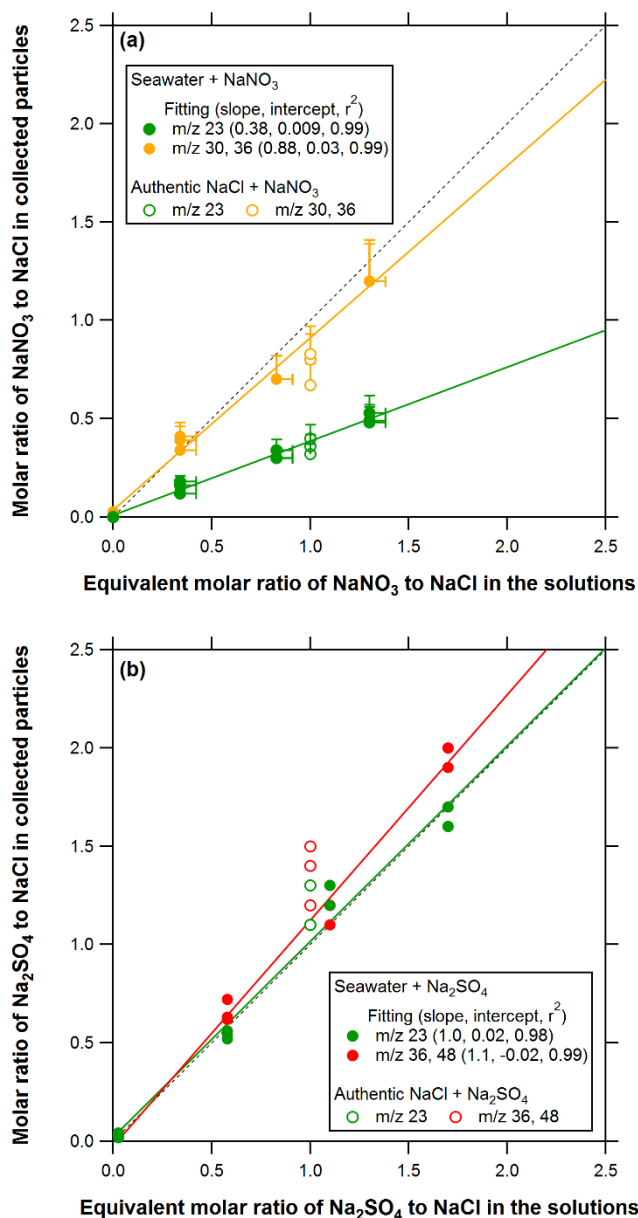
Figure 6. (a) Scatterplots of the molar ratios of SN to SC derived from ion signals versus the equivalent molar ratios of SN to SC in the solutions. The slope, intercept, and r^2 values for the linear regression are indicated in the legend. Solid and open circles represent the data from seawater + SS/SN and authentic SC + SS/SN particles, respectively. The error bars for y-axis represent the uncertainties due to the particle collection efficiencies, whereas those for x-axis represent the uncertainties in estimating the equivalent molar concentrations of the compounds (see the Supplement for details). (b) Same as (a) but for the molar ratios of SS to SC.
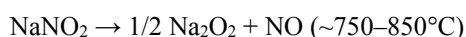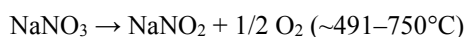
Atmospheric
Measurement
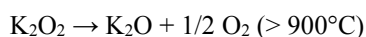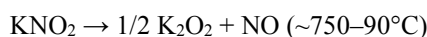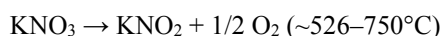Techniques
Discussions

Open Access

EGU

4 Discussion

4.1 Thermal decomposition mechanisms

240   The thermal decomposition mechanisms for SS and PS were discussed by Kobayashi et al. (2021). Here we discuss possible thermal decomposition processes of nitrate and chloride. Tagawa (1987) proposed the following reactions for thermal decomposition of bulk SN in dry air:

$$NaNO_3 \rightarrow NaNO_2 + 1/2\ O_2\ (\sim491\text{--}750°C)$$
$$NaNO_2 \rightarrow 1/2\ Na_2O_2 + NO\ (\sim750\text{--}850°C)$$

245    $$Na_2O_2 \rightarrow Na_2O + 1/2\ O_2\ (> 850°C)$$

and those for PN in dry air:

$$KNO_3 \rightarrow KNO_2 + 1/2\ O_2\ (\sim526\text{--}750°C)$$
$$KNO_2 \rightarrow 1/2\ K_2O_2 + NO\ (\sim750\text{--}90°C)$$
$$K_2O_2 \rightarrow K_2O + 1/2\ O_2\ (> 900°C)$$

250   The observed bimodal peaks at m/z 23 (or 39) originating from SN (or PN) particles could be attributed to the sequentially occurring thermal decomposition of $NaNO_3$ (or KNO_3) and NaO_x (or KO_x).

The thermal decomposition processes of chloride would be simpler than those of nitrate and sulfate. We did not observe significant ion signals at m/z 58 ($Na^{35}Cl^+$) and 74 ($K^{35}Cl^+$). Therefore, SC and PC particles were likely decomposed to metallic and halogen atoms:

255    $$NaCl \rightarrow Na\ (g) + Cl\ (g)$$
$$KCl \rightarrow K\ (g) + Cl\ (g)$$
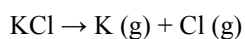
The sensitivity of ion signals at m/z 36 was larger than those at m/z 35 by a factor of ~3. This suggests that Cl (g) evolved from SC/PC particles mostly reacted with H_2O in background air or on the graphite surface to form HCl (g) (Drewnick et al., 2015; Tobler et al., 2020).

260   ### 4.2 Uncertainties in the quantification of single-component particles

The limit of detection (LOD) was estimated as the equivalent concentration at three times the standard deviation (3σ) of the integrated ion signals for repeated ZA measurements (20 samples for each compound). The equivalent concentration is calculated as the ratio of the 3σ value to the product of the sensitivity at a certain m/z and sample air volume. The LOD values estimated by this method are listed in Table 3.

265   The systematic errors due to the particle collection efficiencies were already described in Sect. 2.3. Other systematic errors may originate from the accuracy of the CPC detection efficiency, the DMA sizing, and the flow rate calibrations. These factors are not considered here because they are not specific to the detection of sodium and potassium salts particles by the

Atmospheric
Measurement
Techniques
Discussions

rTDMS. The systematic errors might also originate from the effective density of particles, which was discussed in our previous study (Kobayashi et al., 2021). This factor is not considered because it was difficult to quantify with the current experimental

270 apparatus.

Table 3. Limit of detection (LOD; $\mu g\ m^{-3}$) for the mass concentrations of SN, SC, SS, PN, PC, and PS particles.

	Cation signal (m/z 23, 39)	Anion signal (m/z 30, 36, 48)
SN	0.06	0.5
SC	0.1	0.1
SS	0.1	0.08
PN	0.4	0.4
PC	0.5	0.07
PS	1	0.1

The LODs were estimated as the equivalent concentration at three times the standard deviation (3σ) of the integrated ion signals for repeated ZA measurements with a total measurement cycle of 10 min (particle collection time of 6 min).

275

4.3 Uncertainties in the quantification of multi-component sodium salt particles

The data in Fig. 6 suggest that there are systematic errors in quantifying multi-component sodium salt particles, especially for the SN/SC ratios. This mechanism might be explained by the collection efficiency for multi-component particles. We assume that the collection efficiency for multi-component particles could be approximated as the average of the collection

280 efficiency of the corresponding single-component particles. For seawater (mainly SC) + SS and authentic SC + SS particles, the collection efficiency would be comparable to those of solid SC and SS particles (~70%). For seawater + SN and authentic SC + SN particles, however, the collection efficiency would be in the range of 70–100% (85% as the mid point). Ishizaka et al. (2019) showed that the ERH of equimolar mixed SN and SC particles was ~33%, suggesting that the SN + SC particles (either authentic materials or seawater) were in the solid phase when introduced into the rTDMS. This might explain the

285 underestimation of the SN/SC ratios derived from the m/z 30 and 36 signals.

The deviation of the SN/SC ratios derived from the m/z 23 signals cannot be explained by the systematic errors due to the collection efficiency. We compared the temporal profiles of ion signals at m/z 23 from the single-component SN and SC particles and multi-component SC + SN particles (see the Supplement for details). The ion signals at m/z 23 that could be attributed to SN in the multi-component particles (i.e., the first peak) were smaller than those expected from the single-

290 component SN particles. By contrast, the ion signals at m/z 23 that could be attributed to SC in the multi-component particles (i.e., the second peak) were larger than those from the single-component SC particles. These results suggest that there might be some matrix effects in the quantification of SN and SC particles when using ion signals at m/z 23. Therefore, ion signals at m/z 23 should be used only for qualitative identification of SN and SS particles.

Atmospheric
Measurement
Techniques
Discussions

5 Conclusions and Future Outlook

295   The quantification of sodium and potassium salt (nitrate, chloride, sulfate) particles by the rTDMS was investigated in the laboratory. We generated single-component sodium or potassium salt particles (SN, SC, SS, PN, PC, and PS) and multi-component SN + SC + SS or PN + PC + PS particles. We also generated particles from real seawater samples. The major conclusions are summarized below.

1. Major ion signals originating from single-component sodium or potassium salt particles were clearly detected associated
300   with the increase in the desorption temperature by laser heating. A good linearity ($r^2 > 0.8$) and reproducibility were found between the major ion signals and mass loadings.

2. Temporal profiles of ion signals at m/z 23 (or 39) originating from multi-component sodium (or potassium) salt particles were characterized by three sequential peaks associated with the evolution of the desorption temperature. The first, second, and third peaks were attributed to SN (or PN), SC (or PC), and SS (or PS), respectively.

305 3. Particles generated from seawater samples were used to test the potential interference in the quantification of SS and SN under real-world conditions. Based on the standard addition method, we showed that the ratios of SN (or SS) to SC in collected particles can be quantitatively estimated using the corresponding anion signals (at m/z 30, 36, and 48).

The laboratory experiments demonstrated the proof of concept under well-controlled conditions. Further modifications and tests are needed to deploy the rTDMS for ambient measurement of sea salt and biomass burning aerosols. First, variability in
310 the particle collection efficiencies due to differences in the chemical composition and mixing states should be minimized. The current system achieved collection efficiencies of ~70% for solid sulfate particles, which would also be used for the calibration of the rTDMS during ambient measurement. Ambient particles might be collected with even higher efficiencies if they are in the liquid phase or internally mixed with "sticky" compounds, leading to systematic uncertainties of up to ~30%. Increasing the collection efficiencies for solid particles by improving the geometry of the particle collector may reduce the uncertainties.
315 Second, an alternative ADL for transmitting supermicron particles is desired for measuring ambient sea salt aerosols. Because supermicron ADLs generally require higher operating pressures (Schreiner et al., 1999; Williams et al., 2013), a better differential pumping system may be needed to maintain sufficient vacuum levels for the ion detection.

Author contribution

YK and NT designed the research; YK performed laboratory experiments and data analysis; YK and NT wrote the paper.

References

Adachi, K. and Buseck, P. R.: Changes in shape and composition of sea-salt particles upon aging in an urban atmosphere,
325   Atmos. Environ., 100, 1–9, http://dx.doi.org/10.1016/j.atmosenv.2014.10.036, 2015.

Akagi, S. K., Yokelson, R. J., Wiedinmyer, C., Alvarado, M. J., Reid, J. S., Karl, T., Crounse, J. D., and Wennberg, P. O.:
Emission factors for open and domestic biomass burning for use in atmospheric models, Atmos. Chem. Phys., 11, 4039-
4072, https://doi.org/10.5194/acp-11-4039-2011, 2011.

Andreae, M. O. and Merlet, P.: Emission of trace gases and aerosols from biomass burning, Global Biogeochem. Cycles, 15,
330   4, 955-966, https://doi.org/10.1029/2000GB001382, 2001.

AzadiAghdam, M., Braun, R. A., Edwards, E., Bañaga, P. A., Cruz, M. T., Betito, G., Cambaliza, M. O., Dadashazar, H.,
Lorenzo, G. R., Ma, L., MacDonald, A. B., Nguyen, P., Simpas, J. B., Stahl, C., and Sorooshian, A.: On the nature of sea
salt aerosol at a coastal megacity: Insights from Manila, Philippines in Southeast Asia, Atoms. Environ., 216, 116922,
https://doi.org/10.1016/j.atmosenv.2019.116922, 2019.

335   Broström, M., Enestam, S., Backan, R., and Mäkelä, K.: Condensation in the KCl–NaCl system, Fuel Process. Technol., 105,
142-148, https://doi.org/10.1016/j.fuproc.2011.08.006, 2013.

Chemical Dictionary (1998). Edited by Nagakura, S., Inokuchi, H., Ezawa, H., Iwamura, H., Sato, H., and Kubo, R., Iwanami
Shoten, Publishers, Tokyo, Japan (in Japanese).

Drewnick, F., Diesch, J.-M., Faber, P., and Borrmann, S.: Aerosol mass spectrometry: particle–vaporizer interactions and their
340   consequences for the measurements, Atmos. Meas. Tech., 8, 3811-3830, https://doi.org/10.5194/amt-8-3811-2015, 2015.

Freney, E. J., Martin, S. T., and Buseck, P. R.: Deliquescence and efflorescence of potassium salts relevant to biomass-burning
aerosol particles. Aerosol Sci. Tech 43, 799–807, https://doi.org/10.1080/02786820902946620 , 2009.

Hayes, P. L., Ortega, A. M., Cubison, M. J., Froyd, K. D., Zhao, Y., Cliff, S. S., Hu, W. W., Toohey, D. W., Flynn, J. H., Lefer,
B. L., Grossberg, N., Alvarez, S., Rappenglück, B., Taylor, J. W., Allan, J. D., Holloway, J. S., Gliman, J. B., Kuster, W.
345   C., de Gouw, J. A., Massoli, P., Zhang, X., Liu, J., Weber, R. J., Corrigan, A. L., Russell, L. M., Isaacman, G., Worton, D.
R., Kreisberg, N. M., Goldstein, A. H., Thalman, R., Waxman, E. M., Volkamer, R., Lin, Y. H., Surratt, J. D., Kleindienst,
T. E., Offenberg, J. H., Dusanter, S., Griffith, S., Stevens, P. S., Brioude, J., Angevine, W. M., and Jimenez, J. L.: Organic
aerosol composition and sources in Pasadena, California, during the 2010 CalNex campaign, J. Geophys. Res., 118, 9233–
9257, https://doi.org/10.1002/jgrd.50530, 2013.

350   Hsu, S., Liu, S. C., Kao, S., Jeng, W., Huang, Y., Tseng, C., Tsai, F., Tu, J., and Yang, Y.: Water-soluble species in the marine
aerosol from the northern SouthChina Sea: High chloride depletion related to air pollution, J. Geophys. Res.,112, D19304,
https://doi.org/10.1029/2007JD008844, 2007.

IPCC: Climate Change: 2013. The Physical Science Basis. Contribution of Working Group I to the Fifth Assessment Report
of the Intergovernmental Panel on Climate Change. Stocker, T. F., Qin, D. G.-K. Plattner, M. Tignor, S. K. Allen, J.

Atmospheric
Measurement
Techniques
Discussions

355   Boschung, A. Nauels, Y. Xia, V. Bex, and P. M. Midgley (eds.). Cambridge, United Kingdom: Cambridge University
        Press.

Ishizaka, S., Guo, F., Tian, X., Seng, S., Tobon, Y. A., and Sobanska, S.: In Situ Observation of Efflorescence and
        Deliquescence Phase Transitions of Single NaCl and $NaNO_3$ Mixture Particles in Air Using a Laser Trapping Technique,
        Bull. Chem. Soc. Jpn., 93, 86-91, doi: 10.1246/bcsj.20190285, 2020.

360   Jayne, J. T., Leard, D. C., Zhang, X., Davidovits, P., Smith, K. A., Kolb, C. E., and Worsnop, D. R.: Development of an aerosol
        mass spectrometer for size and composition analysis of submicron particles, Aerosol Sci. Technol., 33, 49–70,
        https://doi.org/10.1246/bcsj.20190285, 2000.

Kerminen, Vwli-Matti, Teinilä, K., Hillamo, R., and Pakkanen, T.: Substitution of chloride in sea-salt particles by inorganic
        and organic anions, J. Aerosol Sci., 29, 929-942, https://doi.org/10.1016/S0021-8502(98)00002-0, 1998.

365   Kobayashi, Y., Ide, Y., and Nobuyuki, T.: Development of a novel particle mass spectrometer for online measurements of
        refractory sulfate aerosols, Aerosol Sci. Technol., 55, 371-386, https://doi.org/10.1080/02786826.2020.1852168, 2021.

Lee, C.-T. and Hsu, W.-C.: The Measurement of Liquid Water Mass Associated with Collected Hygroscopic Waters, J. Aerosol
        Sci., 31, 189-197, https://doi.org/10.1016/S0021-8502(99)00048-8, 2000.

Li, J., Pósfai, M., Hobbs, P. V., and Buseck, P. R.: Individual aerosol particles from biomass burning in southern Africa:2.
370   Compositions   and   aging   of   inorganic   particles,   J.   Geophys.   Res.,   108,   NO.   D13,   8484,
        https://doi.org/10.1029/2002JD002310, 2003.

Miura, K., Kumakura, T., and Sekikawa, T.: The Effect of Continental Air Mass on the Modification of Individual Sea Salt
        Particles   Collected   over   the   Coast   and   the   Open   Sea,   J.   Meteor.   Soc.   Japan,   69,   429–438,
        https://doi.org/10.2151/jmsj1965.69.4_429, 1991.

375   Nakamura, H., Hara, Y., and Osada, H.: The Thermal Decomposition of Ammonium Sulfate and Its Reaction with Iron　(III)
        Oxide, The chemical Society of Japan, 5, 706-710, https://doi.org/10.1246/nikkashi.1980.706, 1980 (in Japanese).

Schlosser, J. S., Braun, R. A., Bradley, T., Dadashazar, H., MacDonald, A. B., Aghdam, M. A., Mardi, A. H., and Sorooshian,
        A.: Analysis of aerosol composition data for western United States wildfires between 2005 and 2015: Dust emissions,
        chloride depletion, and most enhanced aerosol constituents, J. Geophys. Res. Atmos, 122, 8951–8966,
380   https://doi.org/10.1002/2017JD026547, 2017.

Schreiner, J., Schild, U., Voigt, C., and Mauersberger, K.: Focusing of aerosols into a particle beam at pressures from 10 to
        150 Torr, Aerosol Sci. Tech., 31, 373–382, https://doi.org/10.1080/027868299304093, 1999.

Seinfeld, J. H., and S. N. Pandis.: Atmospheric chemistry and physics: From air pollution to climate change. Hoboken N. J:
        Wiley, 2006.

385   Song, J., Zhao, Y., Zhang, Y., Fu, P., Zheng, L., Yuan, Q., Wang, S., Huang, X., Xu, W., Cao, Z., Gromov, S., and Lai, S.:
        Influence of biomass burning on atmospheric aerosols over the western South China Sea: Insights from ions, carbonaceous
        fractions and stable carbon isotope ratios, Environ. Pollut., 248, 1800-1809, https://doi.org/10.1016/j.envpol.2018.07.088,
        2018.

Atmospheric
Measurement
Techniques

Open Access

EGU

Discussions

Tagawa, H.: Thermal Decomposition of Nitrate, Bulletin of the Institute of Environmental Science and Technology, Yokohama
390 National University, 14, 41-57, 1987 (in Japanese).

Takegawa, N., and Sakurai, H.: Laboratory evaluation of a TSI condensation particle counter (Model 3771) under airborne
measurement conditions, Aerosol Sci. Technol, 45, 272–283, https://doi.org/10.1080/02786826.2010.532839, 2011.

Takegawa, N., Miyakawa, T., Nakamura, T., Sameshima, Y., Takei, M., Kondo, Y., and Hirayama, N.: Evaluation of a new
particle trap in a laser desorption mass spectrometer for online measurement of aerosol composition, Aerosol Sci. Technol.,
395 46, 428-443, https://doi.org/10.1080/02786826.2011.635727, 2012.

Tatykaev, B. B., Burkitbayev, M. M., Uralbekov, B. M., and Urakaev, F. KH.: Mechanochemical Synthesis of Silver Chloride
Nanoparticles by a Dilution Method in the System NH_4Cl-$AgNO_3$-NH_4NO_3, Acta Physica Polonica A, 126, doi:
10.12693/APhysPolA.126.1044, 2014.

Tobler, A. K., Skiba, A., Wang, D. S., Croteau, P., Styszko, K., Nęcki, J., Baltensperger, U., Slowik, J. G., and Prévôt, A. S.
400 H.: Improved chloride quantification in quadrupole aerosol chemical speciation monitors (Q-ACSMs), Atmos. Meas. Tech.,
13, 5293–5301, https://doi.org/10.5194/amt-13-5293-2020, 2020.

Weber, R. J., Orsini, D., Daun, Y., Lee, Y. -N., Klotz, P. J., and Brechtel, F.: A particle-into-liquid collector for rapid
measurement of aerosol bulk chemical composition, Aerosol Sci. Technol, 35, 718–27,
https://doi.org/10.1080/02786820152546761, 2001.

405 Williams, L. R., Gonzalez, L. A., Peck, J., Trimborn, D., McInnis, J., Farrar, M. R., Moore, K. D., Jayne, J. T., Robinson, W.
A., Lewis, D. K., Onasch, T. B., Canagaratna, M. R., Trimborn, A., Timko, M. T., Magoon, G., Deng, R., Tang, D., de la
Rosa Blanco, E., Prévôt, A. S. H., Smith, K. A., and Worsnop, D. R.: Characterization of an aerodynamic lens for
transmitting particles greater than 1 micrometer in diameter into the Aerodyne aerosol mass spectrometer, Atmos. Meas.
Tech., 6, 3271–3280, https://doi.org/10.5194/amt-6-3271-2013, 2013.

410 Zauscher, M. D., Wang, Y., Moore, M. J. K., Gaston, C. J., and Prather, K. A.: Air Quality Impact and Physicochemical Aging
of Biomass Burning Aerosols during the 2007 San Diego Wildfires, Environ. Sci. Technol., 47, 14, 7633-7643,
https://doi.org/10.1021/es4004137, 2013.